Original Article

Bioinformatics Prediction of Potential Inhibitors For the SARS-CoV-2 NTPase/Helicase Using Molecular Docking and Dynamics Simulation From Organic Phenolic Compounds

Massoud Saidijam[1], Negin Khaksarimehr[2], Mostafa Rezaei-Tavirani[3], Amir Taherkhani[4*]

Abstract

Background: Coronavirus disease 2019 (COVID-19), caused by the severe acute respiratory syndrome coronavirus 2 (SARS-CoV-2), is a disorder with human-to-human rapid transmission. With several vaccines introduced, we need to find out the effectiveness of such medications in a short-period therapeutic procedure. The NTPase/helicase plays a key role in the replication of the viral RNA.

Materials and Methods: We estimated the binding affinity of several natural polyphenolics, commonly found in fruits and vegetables, with the catalytic site of SARS-CoV-2 helicase by molecular docking analysis using the AutoDock tool. The stability of connections between top-ranked components inside the catalytic site of the helicase was evaluated by molecular dynamics (MD) simulations. The most active residues within the catalytic site of the helicase were ranked based on their degree in a phenolic-residue interaction (PRI) network.

Results: Amentoflavone, theaflavin 3'-gallate, and procyanidin were estimated to be the most potential effective SARS-CoV-2 helicase inhibitors with the salient inhibition constant value (Ki) at the picomolar scale. The docked pose of these compounds was also found to be stable after MD simulations. The binding energy of these compounds with the helicase catalytic site was estimated between −13.90 and −12.77 kcal/mol. Asp534 and Leu412 demonstrated more degrees in the PRI network compared to the other residues.

Conclusion: The present study predicts that amentoflavone, theaflavin 3'-gallate, and procyanidin might be helpful for the treatment of COVID-19.

Keywords: COVID-19, Helicase, Inhibitor, Molecular docking, SARS-CoV-2

1. Department of Molecular Medicine and Genetics, Research Center for Molecular Medicine, Hamadan University of Medical Sciences, Hamadan, Iran
2. School of Pharmacy, Hamadan University of Medical Sciences, Hamadan, Iran
3. Proteomics Research Center, Faculty of Paramedical Sciences, Shahid Beheshti University of Medical Sciences, Tehran, Iran
4. Research Center for Molecular Medicine, Hamadan University of Medical Sciences, Hamadan, Iran

Corresponding Author: Amir Taherkhani, Research Center for Molecular Medicine, Hamadan University of Medical Sciences, Hamadan, Iran.
Tel/Fax: +98-9183145963/8138276299.
Email: a.taherkhani@umsha.ac.ir

Please cite this article as: Saidijam M, Khaksarimehr N, Rezaei-Tavirani M, Taherkhani A. Bioinformatics prediction of potential inhibitors for the SARS-CoV-2 NTPase/helicase using molecular docking and dynamics simulation from organic phenolic compounds. J Cell Mol Anesth. 2021;6(3):222-39. DOI: https://doi.org/10.22037/jcma.v6i3.34490

Introduction

Severe Acute Respiratory Syndrome Coronavirus 2 (SARS-CoV-2), a new form of SARS-CoV, first emerged from Wuhan, China, in December 2019. The corresponding pandemic caused by the SARS-CoV-2 is coronavirus disease 2019 (Covid-19) by the World Health Organization (WHO), which has a fast and wide

transmission. The Covid-19 may lead to severe acute pneumonia in a considerable number of patients, causing organ failure and death (1-3). Although scientists have discovered and introduced several vaccines to diminish the spread of the infection, several complications have remained. For example, mRNA-based vaccines must be stored at −70 degrees Celsius, which may not be possible in common medical centers. Moreover, the production and delivery of vaccines for billions of people around the world have logistical obstacles. Therefore, it is still necessary to discover effective and safe drugs to combat Covid-19 in a short-time therapeutic strategy (4, 5).

A major conserved protein in coronaviruses is NTPase/helicase (NSP13), with a central role in the virus's life cycle. It is responsible for unwinding the double-stranded RNA of the virus by consuming energy from nucleoside triphosphates (6). Therefore, NTPase/helicase has become an attractive target for therapeutic aims in patients affected by coronaviruses (7-12).

In addition to synthesized antiviral drugs (e.g., ribavirin, favipiravir, lopinavir, and ritonavir), which are frequently used against the Covid-19 pandemic (13-15), natural plant-based compounds may serve as an alternative for therapeutic aims in patients affected by SARS-CoV-2 (16-18). Polyphenols (also known as phenolics), the secondary metabolites produced by plants, help elevate the survival of herbs by interacting with unusual environmental conditions such as hazard radiations and pathogens. They are also responsible for many herbal colors (e.g., apples, barriers, and onions). Moreover, phenolic compounds are one of the most abundant molecules found in nutraceutical foods (functional foods), representing several medical and health advantages for treating and preventing disorders. Fruits, vegetables, cereals, olive, legumes, chocolate, and famous beverages such as tea and coffee are the main sources of these natural components. Structurally, they consist of at least one aromatic ring with one or more OH groups (19-24). Phenolics are classified into flavonoids, tannins, phenolic acids, lignans, and stilbenes (25). Flavonoids are the most generous phenolic compounds in daily diet with various pharmacological features, including antioxidant, anti-inflammatory, antibacterial, and antiviral effects (26). The antiviral activity of several flavonoids on DNA and RNA viruses has been confirmed by previous studies (27). For example, it has been demonstrated that apigenin contributes to inhibiting the protein synthesis of picornavirus (RNA virus), leading to an inactive form of the virus (28).

Furthermore, epigallocatechin-3-gallate inhibits DNA replication in herpes simplex, hepatitis B virus, and adenovirus (29). Besides, amentoflavone has illustrated antiviral activity against several viruses (30-32). Therefore, in the present study, it was suggested that polyphenolics contribute to disrupting the normal activity of NTPase/helicase in SARS-CoV-2 via attaching to the catalytic domain of the enzyme.

The present study aimed to perform a drug discovery approach using a molecular docking study to analyze the binding affinity of a total of 52 phenolics (mostly flavonoids) with the catalytic domain of SARS-CoV-2 NTPase/helicase to examine our hypothesis. Identifying compounds with a high affinity of binding to the SARS-CoV-2 catalytic domain may lead to the identification of new drug candidates for the therapeutic aims of Covid-19; Executing molecular dynamics (MD) simulation to examine the resistance of interactions between salient predicted inhibitors and the residues within the SARS-CoV-2 helicase catalytic domain to investigate the stability of docked pose of top inhibitors; Finding the amino acids most efficacious in ligand binding. This was carried out by calculating the degree of each amino acid in the phenolics-residue interaction (PRI) network, which represents the number of interactions between residues and top-ranked inhibitors.

Methods

The Ethics committee approved the present study of Hamadan university of medical sciences, Hamadan, Iran (ethics no. IR.UMSHA.REC.1399.1025). No human/animal was used in this study. The datasets used and/or analyzed during the current study are available from the corresponding author on reasonable request.

Structure preparation: The crystal structure of SARS-CoV-2 helicase was achieved from the Structural Bioinformatics Protein Data Bank (https://www.rcsb.org) as a Protein Data Bank file

(PDB code: 5RLJ) at 1.88 Å X-ray resolution. The 5RLJ file included two chains representing the helicase enzyme, named A and B. Chain B was chosen for molecular docking operations, including 592 residues. Discovery Studio Client version 16.1.0.15350 (https://discover.3ds.com/discovery-studio-visualizer-download) was utilized to minimize the protein's energy (EM). The inhibitor of the helicase in Newman et al.'s study (https://www.rcsb.org/structure/5RLJ), (2S)-2-phenylpropane-1-sulfonamide (PDB code: VW4) was eliminated from the crystal structure before EM. The binding affinity of 52 natural phenolic compounds to the catalytic domain of SARS-CoV-2 helicase was examined. Moreover, vapreotide (PubChem code: 6918026), atazanavir (PubChem code: 148192), ivermectin (PubChem code: 6321424), and scutellarein (PubChem code: 5281697) were considered as control inhibitors of the SARS-CoV-2 helicase. Borgio *et al*. (11) reported that vapreotide and atazanavir (two of the clinically approved drugs against the human immunodeficiency virus [HIV] infection) revealed a considerable binding affinity to the SARS-CoV-2 helicase. This was carried out by a molecular docking study using the MOE software. Besides, Yu *et al*. (12) demonstrated that scutellarein acts as an inhibitor of the SARS-CoV helicase by affecting the ATPase activity of the enzyme *in vitro*. Moreover, Khater *et al*. (33) noted that ivermectin revealed an anti-SARS-CoV-2 helicase activity *in vitro*. Ivermectin has antiparasitic activity and has been approved by the food and drug administration (FDA). The PubChem database (https://pubchem.ncbi.nlm.nih.gov) and the cactus web server (http://cactus.nci.nih.gov/chemical/structure) was utilized to download the structure-data file (SDF) of the compounds and to translate the SDF formats to the PDB files, respectively. The EM for all ligands was performed using the HyperChem software version 8.0.10.

Molecular docking and dynamics simulation: In the present study, we used a windows-based PC to achieve molecular docking and MD simulations. The installed memory, processor, and system type associated with our PC were 32 Gigabytes, Intel Core i7, and 64-bit, respectively. AutoDock software version 4.0 (http://autodock.scripps.edu) and the Discovery Studio Client version 16.1.0.15350 were utilized to study molecular docking and MD simulations. The Lamarckian Genetic Algorithm is the method applied by the AutoDock to locate the compound inside the protonated protein (34-36). After the connection between ligand, the Gibbs free energy of binding ($\Delta G_{binding}$) is estimated by the coming formula (37, 38):

$\Delta G_{binding}$ = Intermolecular Energy + Total Internal Energy + Torsional Free Energy - Unbound System's Energy

The catalytic domain of SARS-CoV-2 helicase was considered as the pocket for docking analysis with phenolic compounds. The grid box options were set to spacing, 0.375 Å; X-dimension, 126; Y-dimension, 124; Z-dimension, 98. The Discovery Studio Client version 16.1.0.15350 was employed to detect the main residues within the helicase catalytic domain.

This was carried out by analyzing the 2-dimensional (2D) view of interactions between the amino acids and small molecules inside the SARS-CoV-2 NTPase/helicase in several studies performed by Newman *et al*. including (2S)-2-phenylpropane-1-sulfonamide (PDB ID: VW4), N-(2-phenylethyl)methanesulfonamide (PDB ID: JFM), 2-(trifluoromethoxy)benzoic acid (PDB ID: K2P), (2S)-2-(4-cyanophenoxy)propanamide (PDB ID: VW1), 1-(propane-2-yl)-1H-imidazole-4-sulfonamide (PDB ID: NYV), 1-(2-ethoxyphenyl)piperazine (PDB ID: H04), 3-(acetylamino)-4-fluorobenzoic acid (PDB ID: NZG), and (3S,4R)-1-acetyl-4-phenylpyrrolidine-3-carboxylic acid (PDB ID: VXG). Accordingly, a total of 27 residues were noticed to be involved in the catalytic domain of the helicase including Arg-129, Leu-132, Phe-133, Asn-177, Ser-264, Gly-285, Thr-286, His-290, Cys-309, His-311, Lys-320, Thy-359, Asn-361, Arg-442, His-482, Ser-485, Ser-486, Ala-487, Ala-505, Trp-506, Tyr-515, Asn-516, Tyr-543, Thy-552, Ala-553, His-554, and Cys-556.

For each component and the control inhibitors, a total of 50 docked configurations were produced. Among all conformations, the one with the most negative $\Delta G_{binding}$ involved in the largest cluster was selected for further analyses, including interaction modes and MD simulation in a period of 500 picoseconds (ps). The interactions between ligands and the helicase enzyme were visualized and analyzed using the BIOVIA Discovery Studio Visualizer version 19.1.0.18287.

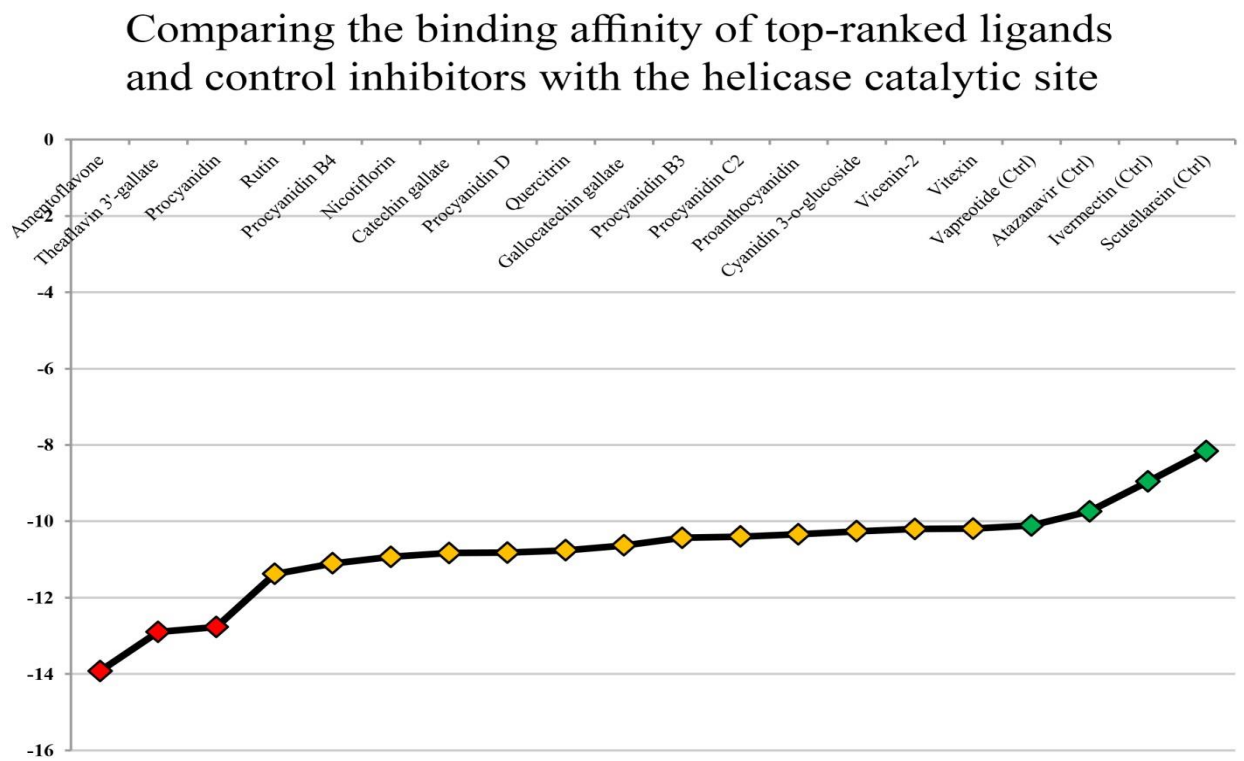

Figure 1. The estimated energy of binding for the top 16 phenolics and control components. X-axis: green diamonds indicate controls. The red ones demonstrate phenolics with the constant inhibition value at the picomolar scale, while the yellow spots represent the other potential inhibitors with the inhibition constant at the nanomolar scale. Y-axis represents the estimated energy of binding (kcal/mol).

Phenolics-residue interaction network: A total of 16 phenolics were predicted as potentially able to connect with the SARS-CoV-2 catalytic site at either nanomolar or picomolar scale with a considerable binding affinity of below −10 kcal/mol. These compounds were considered top-ranked SARS-CoV-2 helicase inhibitors.

The post-docking analysis identified the interacting residues with these top-ranked phenolics. The hole hydrogen, hydrophobic, electrostatic, and miscellaneous interactions between top-ranked inhibitors and their connected residues were illustrated to achieve the PRI network. This was performed using the Cytoscape version 3.8.0.

Results

Molecular docking and molecular dynamics simulations: The binding affinity of several polyphenolics with the SARS-CoV-2 helicase catalytic site was evaluated using an *in silico* approach to combat Covid-19. A total of 16 components had a $\Delta G_{binding}$ value of less than −10 kcal/mol, and therefore, these compounds were noticed to be top-ranked promising inhibitors of SARS-CoV-2 helicase.

Three of them, amentoflavone, theaflavin 3'-gallate, and procyanidin, showed the most considerable inhibition constant value (*K*i), which were calculated to be at the picomolar (pM) scale.

The next 13 inhibitors were estimated to block the catalytic site of the helicase at the nanomolar (nM) scale. Between the control compounds, vapreotide demonstrated the best $\Delta G_{binding}$ and *K*i with the values of −10.11 kcal/mol and 38.98 nM, respectively.

Besides, among top-ranked ligands, vitexin presented the minimum binding affinity to the helicase catalytic site with the $\Delta G_{binding}$ and *K*i value of −10.19 kcal/mol and 33.69 nM. Therefore, the present results show that all the top-ranked phenolics in this study can

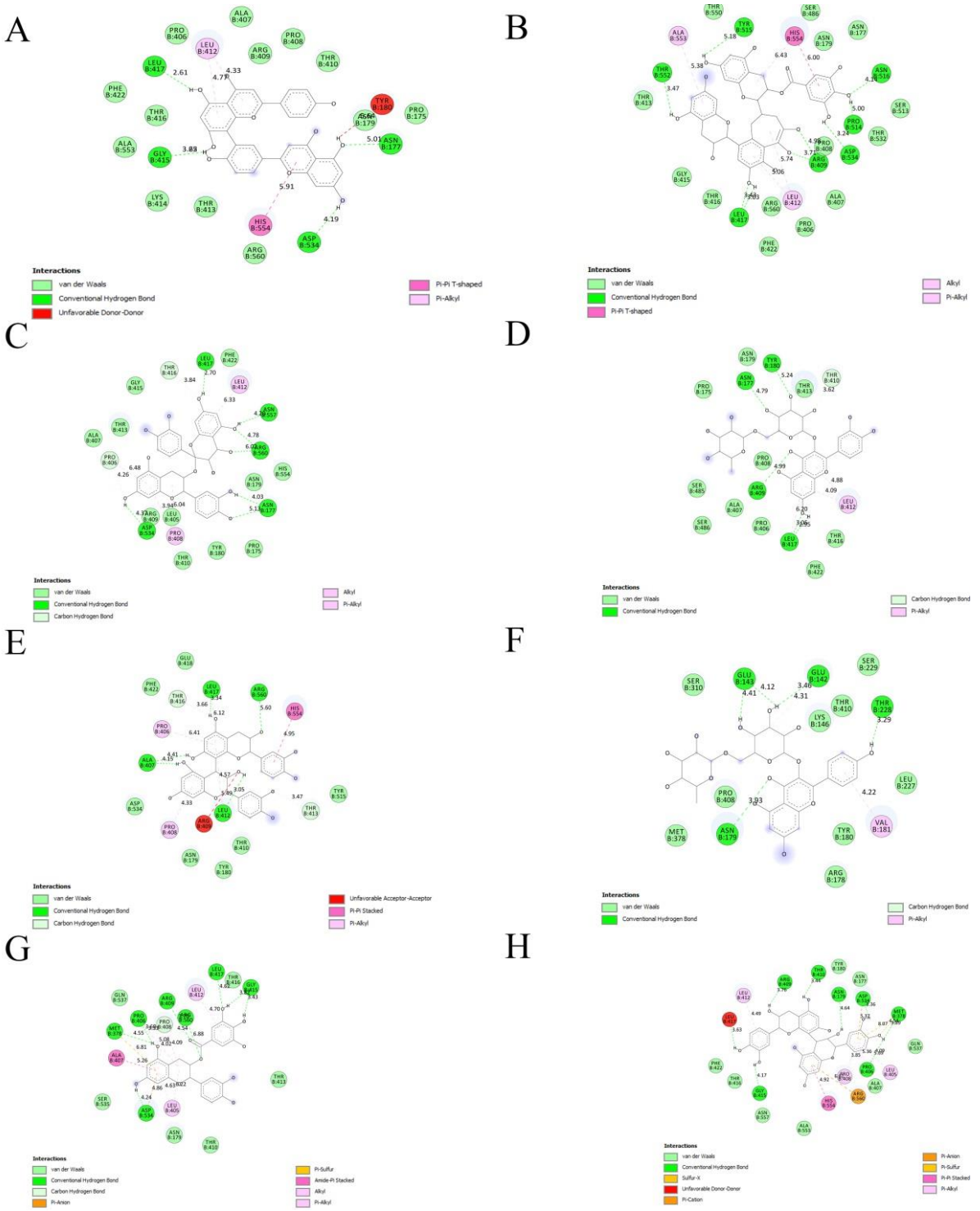

Figure 2. Interaction types after the post docking analysis between SARS-CoV-2 helicase catalytic site and (A) amentoflavone, (B) theaflavin 3'-gallate, (C) procyanidin, (D) rutin, (E) procyanidin B4, (F) nicotiflorin, (G) catechin gallate, (H) procyanidin D, (I) quercitrin, (J) gallocatechin gallate, (K) procyanidin B3, (L) procyanidin C2, (M) proanthocyanidin, (N) cyanidin 3-o-glucoside, (O) vicenin-2, and (P) vitexin.

potentially block the catalytic site of the SARA-CoV-2 helicase more effectively than the control inhibitors *in silico* (Fig. 1). Table 1 demonstrates the $\Delta G_{binding}$ and the *K*i value for all the phenolics and the control inhibitors tested in the present study. The details of energies calculated from the binding of the top-ranked

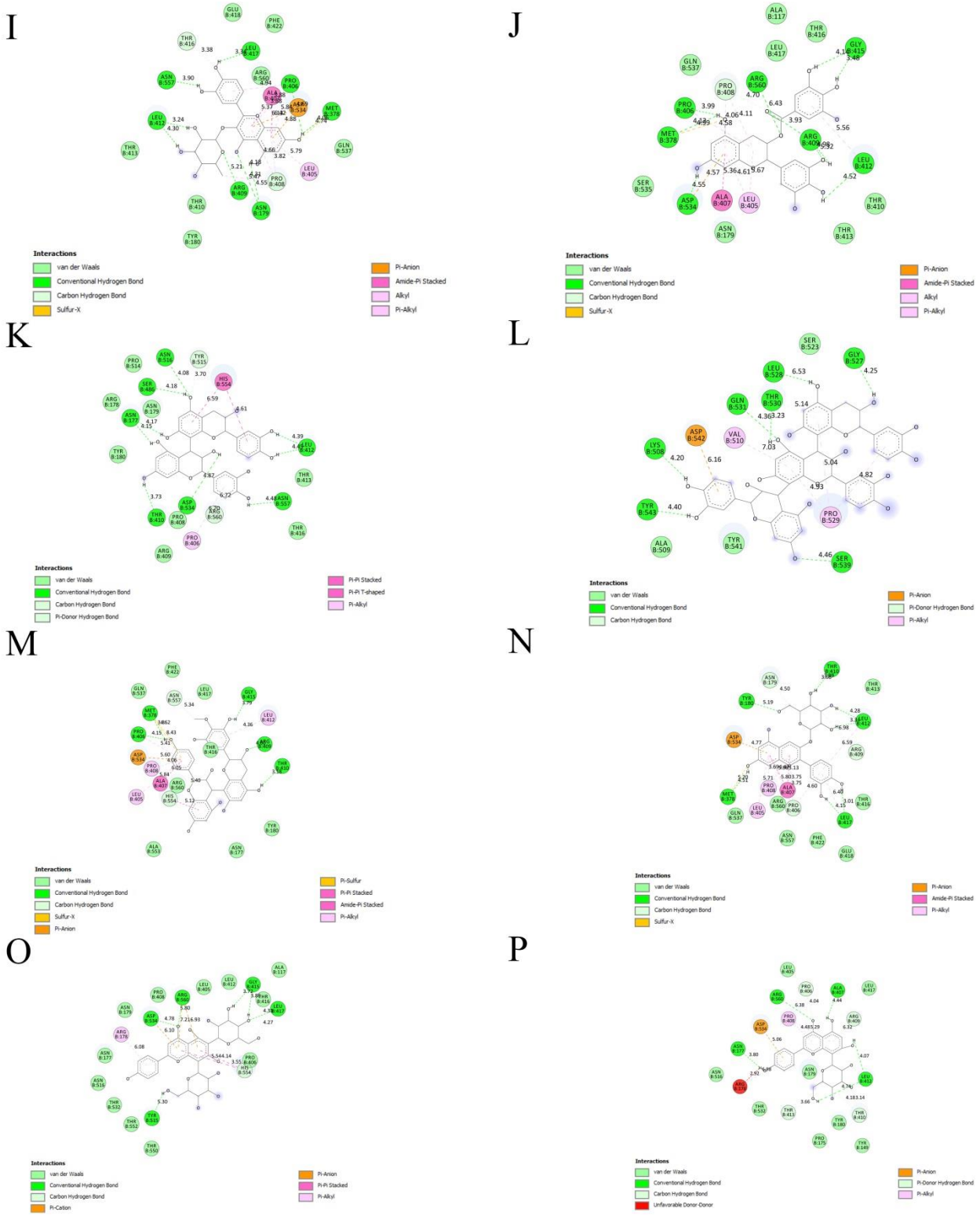

Figure 2. Continued.

components to the SARS-CoV-2 catalytic site, from which the $\Delta G_{binding}$ is calculated, are presented in Table 2. Moreover, after the molecular docking studies analyzed the hydrogen, hydrophobic, electrostatic, and miscellaneous interactions among top-ranked small molecules, control compounds, and the residues within

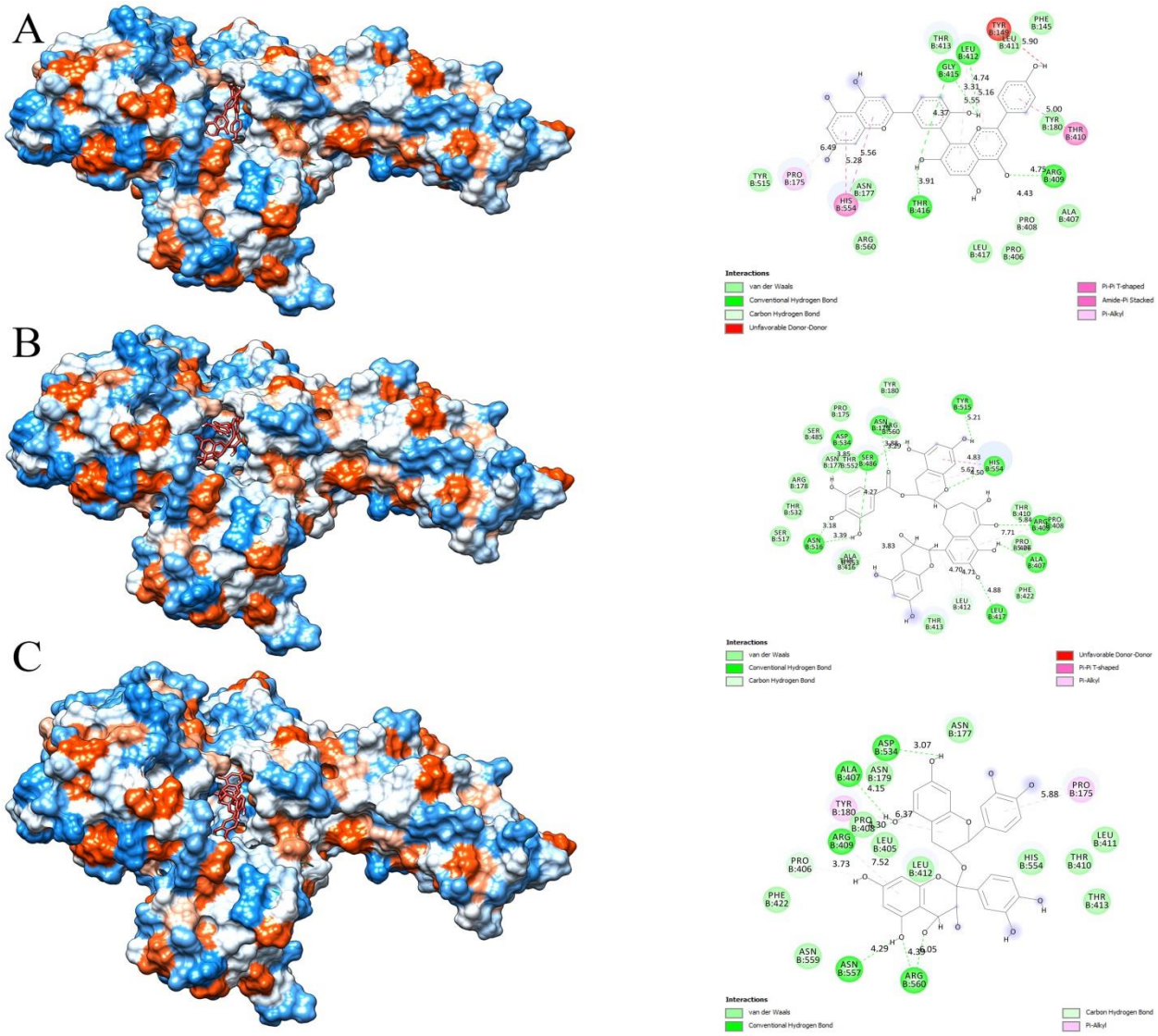

Figure 3. Left figures show three-dimensional position after docking analysis, while the right images illustrate the two-dimensional view of interactions after the MD simulations for (A) amentoflavone, (B) theaflavin 3'-gallate, and (C) procyanidin within the SARS-CoV-2 helicase catalytic site. MD, molecular dynamics.

the helicase catalytic site presented in Table 3. A. The related 2D images for the best 16 phenolics are demonstrated in Fig. 2. MD was simulated to examine the strength of interactions between amentoflavone, theaflavin 3'-gallate, procyanidin, and helicase residues. The interaction modes after the MD simulations are presented in Table 3. B and Fig. 3.

PRI network analysis: A PRI network was constructed with the criteria of 55 nodes, including 16 top-ranked potential inhibitors and 39 residues, and 150 edges (Fig. 4). Each edge shows an interaction between a residue and a component. The number of edges linked to a component was calculated (known as degree) using the Cytoscape software (Fig. 5). It was found that Asp534 and Leu412 had the most interactions with phenolics.

Discussion

The NTPase/helicase is responsible for unwinding the nucleic acid of SARS-CoV-2, leading to genome replication of the virus (12, 39). Accordingly, NSP13 was considered for anti-SARS-CoV-2 drug discovery

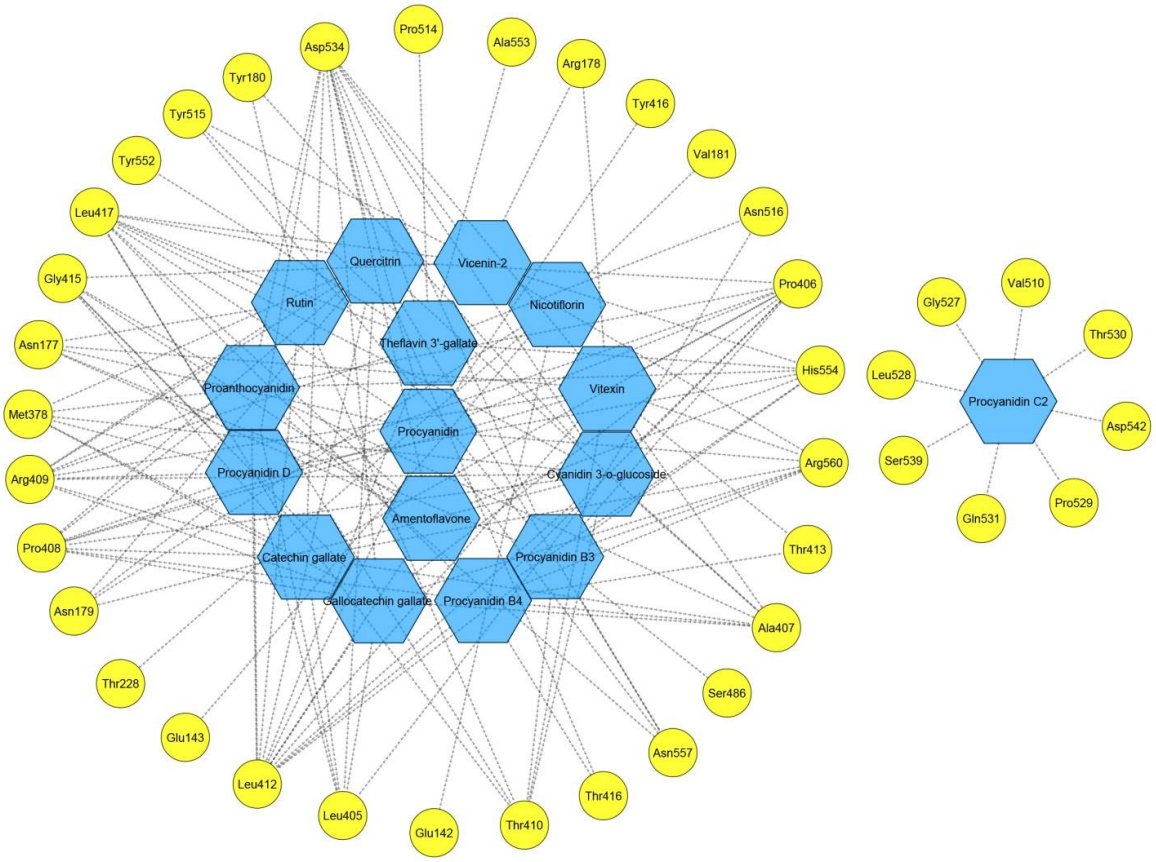

Figure 4. PRI network illustrating interactions among top 16 phenolics and the residues of SARS-CoV-2 helicase catalytic site. PRI, phenolics-residues interaction.

in the current study. A total of 52 natural phenolic compounds were screened for the identification of potential helicase inhibitors. MD was

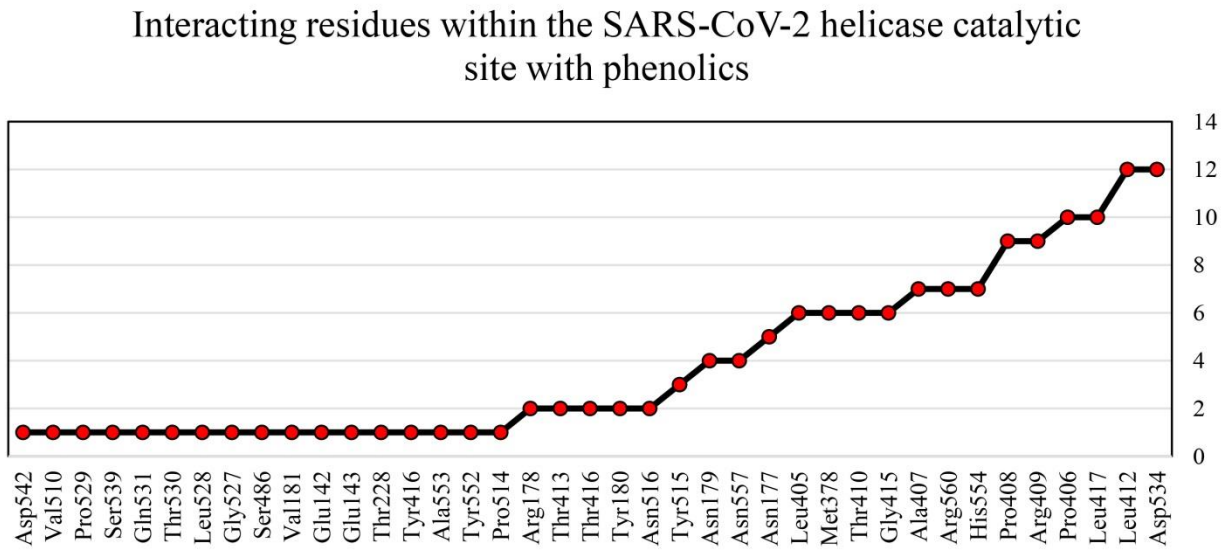

Figure 5. Degree diagram. The X-axis represents the residues within the SARS-CoV-2 helicase catalytic site interacting with the top 16 inhibitors. Y-axis demonstrates the number of interactions for each amino acid.

Table 1: Estimated free energy of binding and inhibition constant values were calculated for the tested natural compounds and the control inhibitors in this study using an *in silico* approach.

PubChem ID	Ligand name	Estimated free energy of binding (kcal/mol)	*Ki*
5281600	Amentoflavone	-13.92	62.72 pM
136825043	Theaflavin 3'-gallate	-12.90	348.75 pM
107876	Procyanidin	-12.77	436.10 pM
5280805	Rutin	-11.38	4.57 nM
147299	Procyanidin B4	-11.10	7.31 nM
5318767	Nicotiflorin	-10.93	9.69 nM
6419835	Catechin gallate	-10.83	11.61 nM
130556	Procyanidin D	-10.82	11.75 nM
5280459	Quercitrin	-10.76	13.04 nM
199472	Gallocatechin gallate	-10.63	16.22 nM
146798	Procyanidin B3	-10.43	22.64 nM
11182062	Procyanidin C2	-10.40	23.61 nM
108065	Proanthocyanidin	-10.34	26.55 nM
441667	Cyanidin 3-o-glucoside	-10.26	30.09 nM
442664	Vicenin-2	-10.20	33.59 nM
5280441	Vitexin	-10.19	33.69 nM
122738	Procyanidin B2	-9.96	50.36 nM
5280704	apigenin-7-glucoside	-9.88	47.97 nM
5280804	Isoquercitrin	-9.87	58.01 nM
124017	Procyanidol B5	-9.60	92.38 nM
124052	glabridin	-9.37	134.67 nM
5281675	orientin	-9.37	136.45 nM
5353915	Quercetin-3-rhamnoside	-9.21	176.55 nM
474541	Procyanidin B8	-9.17	188.37 nM
124025	Procyanidin A2	-8.93	282.96 nM
5318997	Icariin	-8.24	918.46 nM
94672	Sesaminol	-8.13	1.10 uM
5281654	Isorhamnetin	-7.91	1.60 uM
5280445	Luteolin	-7.89	1.64 uM
72277	Epigallocatechin	-7.89	1.64 uM
638278	Isoliquiritigenin	-7.80	1.93 uM
101612	Asarinin	-7.75	2.10 uM
86289522	baicalein(1-)	-7.69	2.29 uM
5280443	apigenin	-7.69	2.32 uM
1203	Epicatechin	-7.59	2.72 uM
5280343	Quercetin	-7.54	2.97 uM

5281607	Chrysin	-7.53	3.00 uM
629440	Hemileiocarpin	-7.52	3.06 uM
5280863	Kaempferol	-7.51	3.11 uM
439533	taxifolin	-7.49	3.26 uM
65084	Gallocatechin	-7.42	3.61 uM
5281672	Myricetin	-7.36	963.30 nM
5318998	licochalcone a	-7.32	4.27 uM
9064	Catechin	-7.30	4.45 uM
72307	sesamin	-7.28	4.58 uM
14309735	Xanthogalenol	-7.25	4.88 uM
72344	Nobiletin	-7.19	5.37 uM
443639	Epiafzelechin	-7.02	7.14 uM
12241084	Daidzein-3',5',8-d3	-6.74	11.49 uM
145858	Flavylium	-6.73	11.62 uM
5280378	Formononetin	-6.59	14.85 uM
5280544	Herbacetin	-6.54	16.01 uM
6918026	Vapreotide (Ctrl)	-10.11	38.98nM
148192	Atazanavir (Ctrl)	-9.74	72.68 nM
6321424	Ivermectin (Ctrl)	-8.96	268.85 nM
5281697	Scutellarein (Ctrl)	-8.16	1.05 uM

*K*i, inhibition constant.

also simulated for top-ranked inhibitors. The results of the present study are important due to several reasons:

- First, a total of 16 plant-based compounds were estimated to attach the SARS-CoV-2 catalytic domain more tightly than the control inhibitors
- Second, it was predicted that amentoflavone, theaflavin 3'-gallate, and procyanidin can block the SARS-CoV-2 catalytic domain at the picomolar concentration, which is not always achievable by molecular docking analysis.

In addition, the docked pose of these compounds was found to be stable in the simulation on the 500 ps time scale. Moreover, herbal inhibitors have advantages compared to synthetic compounds due to availability, low price, and safety aspects, to name a few (40).

Experimental approaches have previously demonstrated the anti-SARS-CoV NTPase/helicase activity of several flavonoids. Quercetin has been reported to be a potent inhibitor of SARS-CoV NTPase/helicase; the half-maximal inhibitory concentration (IC_{50}) of quercetin against the unwinding activity of the enzyme was reported to be 8.1 μM. This was performed by applying the recombinant helicase and a fluorescence resonance energy transfer (FRET)-based assay (41).

Moreover, Park *et al.* (42) demonstrated the anti-SARS-CoV NTPase/helicase activity of several derivatives of 7-O-aryl-methyl quercetin; the IC_{50} of the compounds were reported from 2.7 to 5.2 μM.

According to a study by Yu et al. (12), scutellarein and myricetin have displayed anti-ATPase activity against the SARS-CoV helicase with IC50 values of 0.86 and 2.71 μM, respectively. In the present study, it was estimated that quercetin and quercetin-3-rhamnoside could connect to the catalytic domain of SARS-CoV-2 NTPase/helicase with the $\Delta G_{binding}$ of −7.54 and −9.21 kcal/mol, respectively, while the estimated energy of binding between myricetin and SARS-CoV-2 NTPase/helicase was −7.36 kcal/mol.

Table 2: Details of energies for the top 16 ligands from which the estimated energy of binding is calculated.

Ligand name	Final intermolecular energy (kcal/mol)	Final total internal energy (kcal/mol)	Torsional free energy (kcal/mol)	Unbound system's energy (kcal/mol)	Estimated free energy of binding (kcal/mol)
Amentoflavone	-11.88	-6.1	2.68	-1.38	-13.92
Theaflavin 3'-gallate	-13.12	-6.71	4.77	-2.16	-12.90
Procyanidin	-12.14	-6.43	4.18	-1.62	-12.77
Rutin	-8.88	-9.38	4.77	-2.11	-11.38
Procyanidin B4	-11.18	-5.64	3.88	-1.84	-11.10
Nicotiflorin	-8.87	-8.61	4.47	-2.08	-10.93
Catechin gallate	-10.48	-4.9	3.28	-1.28	-10.83
Procyanidin D	-12.49	-3.93	3.88	-1.72	-10.82
Quercitrin	-11.57	-3.54	2.98	-1.38	-10.76
Gallocatechin gallate	-10.86	-4.76	3.58	-1.42	-10.63
Procyanidin B3	-11.52	-4.79	3.88	-2.01	-10.43
Procyanidin C2	-11.51	-8.54	5.97	-3.68	-10.40
Proanthocyanidin	-12.01	-3.92	3.88	-1.72	-10.34
Cyanidin 3-o-glucoside	-11.79	-3.45	3.58	-1.41	-10.26
Vicenin-2	-9.88	-7.55	4.77	-2.46	-10.20
Vitexin	-9.47	-4.84	2.98	-1.13	-10.19
Vapreotide (Ctrl)	-9.87	-6.5	4.18	-2.09	-10.11
Atazanavir (Ctrl)	-10.09	-4.93	3.58	-1.71	-9.74
Ivermectin (Ctrl)	-9.17	-1.19	0.89	-0.5	-8.96
Scutellarein (Ctrl)	-8.16	0	0	0	-8.16

Black tea is a well-known beverage obtained from the leaves of the *Camellia sinens* containing a considerable number of orange-red pigments, which are the rich sources of theaflavins (TFs) such as theaflavin, theaflavin-3-gallate, and theaflavin-3,3′-digallate with many valuable health effects. Previous studies have reported antioxidant and pro-oxidant properties for TFs, leading to tumorigenesis prevention and selective cytotoxicity against cancer cells, respectively (43-49). Our results estimated that theaflavin 3'-gallate could bind to the SARS-CoV-2 helicase catalytic site at the picomolar scale (*K*i = 348.75 pM) with a considerable $\Delta G_{binding}$ of −12.90 kcal/mol. Furthermore, before MD simulation, theaflavin 3'-gallate exhibited nine hydrogens and five hydrophobic interactions with Arg409, Leu412, Leu417, Pro514, Tyr515, Asn516, Asp534, Tyr552, Ala553, and His554 residues within the helicase catalytic site. In comparison, this compound illustrated thirteen hydrogens and four hydrophobic interactions with the Asn179, Ala407, Arg409, Leu412, Thr416, Leu417, Ser486, Tyr515, Asn516, Asp534, and His554 amino acids within the helicase catalytic site, after the MD simulation. Of note, a π-π stack pairing was found between His554 and theaflavin 3'-gallate before and after MD simulations with the length of 6.00 Å and 4.83 Å, respectively. The π-π stack pairing is the main interaction mode between drugs and proteins, which creates a stable drug-protein connection (37). Clark *et al*. (50) reported that the combination of theaflavin, theaflavin-3-monogallate, theaflavin-3′-monogallate, and theaflavin-3,3′digallate revealed anti-bovine coronavirus (BCV) activity with the criteria of mean effective concentration (EC_{50}) = 34.7 μg/ml. These authors used the HRT-18 cell line for their experiments. Lung *et al*. (51) designed a study to

Table 3: Different types of interactions between the top inhibitors in this study and SARS-CoV-2 catalytic site residues.

A, Before molecular dynamics simulations

Ligand name	Hydrogen bond (distance Å)	Hydrophobic interaction (distance Å)	Electrostatic (distance Å)	Miscellaneous (distance Å)
Amentoflavone	Asn177 (5.01: classical); Asp534 (4.19: classical); Gly415 (3.55*: classical); Leu417 (2.61: classical)	His554 (5.91*: pi); Leu412 (4.33*: mixed, 4.77*: mixed)	NA	NA
Theaflavin 3'-gallate	Tyr515 (5.18*: classical); Asn516 (4.14*: classical); Pro514 (5.00: classical); Asp534 (3.24*: classical); Arg409 (3.71*: classical, 4.98: classical); Leu417 (3.03*: classical, 3.43: classical); Tyr552 (3.47: classical);	His554 (6.00*: pi, 6.43*: mixed); Leu412 (5.06*: mixed); Ala553 (5.38: mixed, 5.44*: alkyl);	NA	NA
Procyanidin	Thr416 (3.84: non-classical); Leu417 (2.70: classical); Asn557 (4.20*: classical); Arg560 (4.78*: classical, 6.02*: classical); Asn177 (4.03: classical, 5.13: classical); Asp534 (4.37*: classical); Pro406 (4.26*: non-classical)	Leu412 (6.33: mixed); Pro408 (3.94: mixed, 6.04: alkyl); Pro406 (6.48: mixed)	NA	NA
Rutin	Tyr180 (5.24); Asn177 (4.79); Thr410 (3.62); Arg409 (4.99); Leu417 (2.95,3.06)	Leu417 (6.20); Leu412 (4.09,4.88)	NA	NA
Procyanidin B4	Ala407 (4.15,4.41); Thr416 (3.66); Leu417 (3.34); Arg560 (5.60); Thr413 (3.47); Leu412 (3.05)	His554 (4.95); Leu417 (6.12); Pro406 (6.41); Leu412 (4.57); Pro408 (4.33)	NA	NA
Nicotiflorin	Asn179 (3.93); Thr228(3.29); Glu143 (4.12,4.41); Glu142 (3.46,4.31)	Val181 (4.22)	NA	NA
Catechin gallate	Asp534 (4.24); Met378 (4.55); Pro406 (3.33,3.60); Pro408 (4.54); Arg409 (3.70); Arg560 (6.88); Leu417 (4.62); Gly415 (3.43,3.82)	Ala407 (5.34); Pro408 (4.06,4.11); Leu405 (4.61,5.67); Leu412 (5.56); Pro406 (4.58)	Asp534 (4.86)	Met378 (6.81)
Procyanidin D	Gly415 (4.17); Leu417 (3.63); Arg409 (3.76); Thr410(3.44); Asn179(4.64); Asp534 (3.36); Met378 (3.89); Pro406 (4.09)	Leu412 (4.49); His554 (4.92); Pro406 (5.36); Pro408 (3.85); Leu405 (5.69)	Arg560 (6.61); Asp534 (5.37)	Met378 (4.54,8.07)
Quercitrin	Met378 (4.06); Pro406 (3.88,4.69); Leu417 (3.34); Thr416 (3.38); Asn557 (3.90); Leu412 (3.24,4.30); Arg409 (5.21); Asn179 (4.55,5.47); Pro408 (4.18)	Pro406 (3.88,4.94,5.84); Ala407 (5.37,6.13); Pro408 (3.82,4.31,4.66); Leu405 (5.79)	Asp534 (4.88,6.42)	Met378 (4.74)

Gallocatechin gallate	Gly415 (3.48,4.14); Arg560 (6.43); Arg409 (3.93,4.98,5.32); Pro408 (4.70); Pro406 (3.99); Met378 (4.12); Asp534 (4.55); Leu412 (4.52)	Pro408 (4.06,4.11); Pro406(4.58); Leu405 (4.61,5.67); Ala407 (5.36); Leu412 (5.56)	Asp534(4.57)	Met378 (4.99)
Procyanidin B3	Tyr515 (3.70); Asn516 (4.08); Ser486 (4.18); Asn177 (4.15,4.17); Thr410 (3.73); Asp534 (4.87); Arg560 (6.72); Asn557 (4.48); Leu412 (4.39,4.45)	His554 (4.61,6.59); Pro406 (6.70)	NA	NA
Procyanidin C2	Gly527 (4.25); Leu528 (6.53); Thr530 (3.23,5.14); Gln531 (4.36); Ser539 (4.46)	Pro529 (4.82,4.93,5.04); Val510 (7.03)	Asp542 (6.16)	NA
Proanthocyanidin	His554 (5.40); Thr410 (3.18); Arg409 (4.60); Pro406 (4.15); Met378 (3.86); Asn557 (5.34); Gly415 (3.79)	Leu412 (4.36); His554 (5.12); Leu405 (5.84); Ala407 (6.05); Pro408 (4.06); Pro406 (5.41)	Asp534 (5.60)	Met378 (4.62,8.43)
Cyanidin 3-o-glucoside	Leu412 (3.34,4.28); Arg409 (6.98); Thr410 (3.68,3.89); Asn179 (4.50); Tyr180 (5.19); Met378 (4.51); Pro406 (3.75); Leu417 (3.01,4.15)	Leu405 (5.71); Pro408 (3.69,4.47); Ala407 (5.13,5.98); Pro406 (3.75,4.60,5.80); Leu412 (6.59); Leu417 (6.40)	Asp534 (4.77)	Met378 (5.20)
Vicenin-2	Leu417 (4.27,4.31); Gly415 (3.72,3.86); Arg560 (5.80); Asp534 (4.78); Tyr515 (5.30); His554 (3.55)	His554 (4.14,5.54); Arg178 (6.08)	Asp534 (6.10); Arg560 (6.93,7.21)	NA
Vitexin	Thr410 (3.14,4.18); Thr413 (3.66); Leu412 (4.07,4.74); Arg409 (6.32); Asn177 (3.80); Ala407 (4.44); Pro406 (4.04); Arg560 (6.38)	Pro408 (4.48,5.29); Arg409 (6.32); Arg178 (6.98)	Asp534 (5.06)	NA
Atazanavir (Ctrl)	Phe343 (5.87); Cys342 (4.25); Lys345 (5.55); Ala312 (2.97); Asp315 (4.36); Ser539 (4.03)	Ala312 (4.27,4.94); Ala313 (5.58); Ala316 (5.51); Cys342 (4.81)	Lys345 (5.55); Glu319 (4.30)	NA
Vapreotide (Ctrl)	Gln531 (3.59); Cys342 (4.43); Asp315 (4.92); Arg178 (3.46); Glu201 (5.51,5.58)	Arg178 (4.62,5.13,5.71,5.84); Ala312 (4.10)	NA	NA
Ivermectin (Ctrl)	Tyr541 (4.30); Asp542 (3.30); Lys569 (5.48); Glu319 (4.28); Lys345 (5.19,5.87)	Tyr541 (6.28); Val510 (5.03); Pro529 (6.16)	NA	NA

Scutellarein (Ctrl)	Asp534 (5.39); Asn179 (5.29); Thr416 (3.37); Leu417 (3.72)	Pro46 (3.89,4.97,5.80); Leu417 (6.32); Leu405 (5.82); Pro408 (3.80,4.74); Ala407 (5.43,6.10); Leu412 (6.42)	Asp534 (4.98)	Met378 (4.90)
B, After molecular dynamics simulations				
Ligand name	**Hydrogen bond (distance Å)**	**Hydrophobic interaction (distance Å)**	**Electrostatic (distance Å)**	**Miscellaneous (distance Å)**
Amentoflavone	Leu412 (4.74: classical); Gly415 (3.31: classical, 4.37: classical); Thy416 (3.91: classical); Arg409 (4.75: classical;); Pro408 (4.43: non-classic)	Thr410 (5.00: pi); His554 (5.28: pi, 5.56: pi); Pro175 (6.49: mixed); Leu412 (5.16: mixed, 5.55: mixed)	NA	NA
Theaflavin 3'-gallate	Tyr515 (5.21: classical); His554 (4.50: classical); Arg409 (5.84: classical); Ala407 (5.26: classical); Leu417 (4.88: classical); Asn516 (3.18: classical, 3.39: classical); Ser486 (3.29: classical, 4.27: classical); Asp534 (3.85:' classical); Asn179 (3.88: classical); Leu412 (4.70: non-classical); Thr416 (3.83: non-classical)	His554 (4.83: pi, 5.62: mixed, 5.80: mixed); Arg409 (7.71: mixed); Leu412 (4.71: mixed); Ala553 (6.61: alkyl)	NA	NA
Procyanidin	Asp534 (3.07: classical); Ala407 (4.15: classical); Arg409 (4.30: classical); Pro406 (3.73: non-classical); Asn557 (4.29: classical); Arg560 (4.39: classical, 6.05: classical)	Pro175 (5.88: mixed); Tyr180 (6.37: mixed); Arg409 (7.52: mixed)	NA	NA

The asterisks (*) show the interactions that were found to be stable after MD simulations. MD, molecular dynamics; NA, not available.

evaluate the binding affinity of several traditional Chinese medicinal compounds with the catalytic site of RNA-dependent RNA polymerase (RdRp) in SARS-CoV SARS-CoV-2, and Middle East respiratory syndrome coronavirus (MERS-CoV) using the idock protein-ligand docking tool (https://GitHub.com/HongjianLi/idock). The authors reported that theaflavin revealed binding energy of −9.11 kcal/mol, −8.03 kcal/mol, and −8.26 kcal/mol with the RdRp of SARS-CoV-2, SARS-CoV, and MERS-CoV, respectively.

Amentoflavone is a biflavone metabolite with several health benefits, including antioxidative, anti-inflammatory, anticancer, antimicrobial, neuroprotective, and anti-radiational characteristics (52-63). According to the present results, it was estimated that amentoflavone could attach to the catalytic site of SARS-CoV-2 helicase at the picomolar scale (*K*i = 62.72 pM) with an outstanding $\Delta G_{binding}$ of −13.92 kcal/mol. Before MD simulation, amentoflavone formed four hydrogens, three hydrophobic and one unfavorable interaction with Asn177, Tyr180, Leu412, Gly415, Leu417, Asp534, and His554 residues inside the helicase catalytic site. In comparison, this ligand showed six hydrogens and six hydrophobic interactions with Pro175, Pro408, Arg409, Thy410, Leu412, Gly415, Tyr416, and His554 residues inside the helicase catalytic site after the MD simulation. A π-π stack pairing was detected between amentoflavone and His554 (5.91 Å) before MD simulation, while after the MD simulation, amentoflavone demonstrated one and two π-π stack pairing interactions with the Thr410 (5.00 Å) and His554 (5.28 Å, 5.56 Å), respectively. Ryu *et al.* (64) conducted a study to examine the anti-SARS-CoV $3CL^{Pro}$ activity of *Torreya nucifera* leaves extracts, which is widely used in traditional medicine in Asia. The authors reported that amentoflavone had the strongest inhibitory effect among the extract components on the $3CL^{Pro}$ activity with an IC_{50} and *K*i value of 8.3 μM and 13.8 μM, respectively: this was carried out using the fluorescence resonance energy

transfer (FRET) and molecular docking analysis. Several plants have been identified as the rich sources of amentoflavone, such as *Ginkgo biloba, Selaginella tamariscina, Juniperus communis L, Hypericum perforatum,* and *Biophytum sensitivum* (65-68).

Procyanidins are the most abundant subgroup of flavonoids with many pharmaceutical properties including antioxidant, anti-inflammatory, antitumor, and cardioprotective effects. Structurally, they consist of two monomers of catechins and epicatechins forming dimers, trimers, tetramers, or more massive molecules. These metabolites are mainly found in grape juice, grape seed, apple, and cocoa (69-74). Zhuang *et al*. (75) studied the antiviral activity of butanol fraction obtained from the *Cinnamomi Cortex* on the wild-type of SARS-CoV (wtSARS-CoV). The authors demonstrated that procyanidin A2 and procyanidin B1 had a mild effect on the activity of wtSARS-CoV with an IC_{50} value between 30 and 40 µM. This was carried out using the plaque reduction assay. Based on our findings, it was predicted that procyanidin could considerably connect to the SARS-CoV-2 helicase catalytic site at the picomolar scale (*K*i = 436.10 pM) with a $\Delta G_{binding}$ of −12.77 kcal/mol. Moreover, before MD simulation, procyanidin exhibited nine hydrogens and four hydrophobic interactions with Asn177, Pro406, Pro408, Leu412, Tyr416, Leu417, Asp534, Asn557, and Arg560 residues within the helicase catalytic site. In comparison, this component demonstrated seven hydrogens and three hydrophobic interactions with the Pro175, Tyr180, Pro406, Ala407, Arg409, Asp534, Asn557, and Arg560 residues inside the helicase catalytic site after the MD simulation. It was also predicted that procyanidin B4, procyanidin D, procyanidin B3, procyanidin C2, proanthocyanidin, procyanidin B2, procyanidin B5, procyanidin B8, and procyanidin A2 could attach to the SARS-CoV-2 helicase catalytic site at the nanomolar scale with the $\Delta G_{binding}$ ranging from −11.10 (for procyanidin B4) to −8.93 kcal/mol (for procyanidin A2).

Based on MD simulations, it was found that amentoflavone illustrated four stable interactions with the SARS-CoV-2 helicase catalytic domain, including one hydrogen and three hydrophobic interactions. Also, theaflavin 3'-gallate formed nine stable interactions with the residues within the enzyme including five hydrogens and four hydrophobic interactions. Moreover, procyanidin demonstrated five hydrogen bonds with the amino acids inside the SARS-CoV-2 helicase. Therefore, the docked pose of amentoflavone, theaflavin 3'-gallate, and procyanidin was revealed to be stable, suggesting that these compounds could be considered as potentially effective inhibitors of the SARS-CoV-2 NTPase/helicase and may disrupt the unwinding process of the viral RNA. The three-dimensional docked pose of amentoflavone, theaflavin 3'-gallate, and procyanidin after MD simulations are illustrated in Fig. 3.

There are some limitations in the present study. No supercomputer was available for the research team to perform MD simulations. Besides, the helicase enzyme within the 5RLJ file contained 592 residues. Therefore, the MD simulation was time-consuming for the research team and took several days to complete the MD simulation for each ligand-protein complex. Performing MD simulation for greater time scales is suggested in future studies, although it needs faster processors *in silico*. It is also suggested that MD simulation be applied for other top-ranked compounds in this study to reveal more potentially effective inhibitors of SARS-CoV-2 helicase. Furthermore, wet-lab experiments are required to confirm our findings.

Conclusion

In summary, the present study suggests that amentoflavone, theaflavin 3'-gallate, and procyanidin could be considered potentially effective inhibitors of the enzyme, leading to disruption in the viral RNA replication. This was carried out using molecular docking and dynamics simulations. Besides, Asp534 and Leu412 were the most active amino acids within the catalytic domain of the enzyme. However, *in vitro* and *in vivo* analyses are required to validate these findings.

Acknowledgment

The authors would like to appreciate the Deputy of Research and Technology and Research Center for Molecular Medicine, Hamadan University of Medical

Sciences, Hamadan, Iran, for their support; the Grant No. was 9912128940 and the research proposal was approved by the Hamadan University of Medical Scieneces (Ethics Committee), with this egistration code: IR.UMSHA.REC.1399.1025.

Conflicts of Interest

The authors declare that they have no conflict of interest.

References

1. Zhou MY, Xie XL, Peng YG, Wu MJ, Deng XZ, Wu Y, et al. From SARS to COVID-19: What we have learned about children infected with COVID-19. Int J Infect Dis. 2020;96:710-4.
2. Dhillon P, Breuer M, Hirst N. COVID-19 breakthroughs: separating fact from fiction. FEBS J. 2020;287(17):3612-32.
3. Iba T, Levy JH, Levi M, Thachil J. Coagulopathy in COVID-19. J Thromb Haemost. 2020;18(9):2103-9.
4. Horby P, Lim WS, Emberson JR, Mafham M, Bell JL, Linsell L, et al. Dexamethasone in Hospitalized Patients with Covid-19. N Engl J Med. 2021;384(8):693-704.
5. Izda V, Jeffries MA, Sawalha AH. COVID-19: A review of therapeutic strategies and vaccine candidates. Clin Immunol. 2021;222:108634.
6. Ziebuhr J. The coronavirus replicase. Curr Top Microbiol Immunol. 2005;287:57-94.
7. Keum YS, Jeong YJ. Development of chemical inhibitors of the SARS coronavirus: viral helicase as a potential target. Biochem Pharmacol. 2012;84(10):1351-8.
8. Ivanov KA, Thiel V, Dobbe JC, van der Meer Y, Snijder EJ, Ziebuhr J. Multiple enzymatic activities associated with severe acute respiratory syndrome coronavirus helicase. J Virol. 2004;78(11):5619-32.
9. Adedeji AO, Lazarus H. Biochemical Characterization of Middle East Respiratory Syndrome Coronavirus Helicase. mSphere. 2016;1(5).
10. Wong SS, Yuen KY. The severe acute respiratory syndrome (SARS). J Neurovirol. 2005;11(5):455-68.
11. Umadevi P, Manivannan S, Fayad AM, Shelvy S. In silico analysis of phytochemicals as potential inhibitors of proteases involved in SARS-CoV-2 infection. J Biomol Struct Dyn. 2020:1-9.
12. Yu MS, Lee J, Lee JM, Kim Y, Chin YW, Jee JG, et al. Identification of myricetin and scutellarein as novel chemical inhibitors of the SARS coronavirus helicase, nsP13. Bioorg Med Chem Lett. 2012;22(12):4049-54.
13. Varga Z, Flammer AJ, Steiger P, Haberecker M, Andermatt R, Zinkernagel AS, et al. Endothelial cell infection and endotheliitis in COVID-19. Lancet. 2020;395(10234):1417-8.
14. Magro G. COVID-19: Review on latest available drugs and therapies against SARS-CoV-2. Coagulation and inflammation cross-talking. Virus Res. 2020;286:198070.
15. Johnson RM, Vinetz JM. Dexamethasone in the management of covid -19. BMJ. 2020;370:m2648.
16. Wahedi HM, Ahmad S, Abbasi SW. Stilbene-based natural compounds as promising drug candidates against COVID-19. J Biomol Struct Dyn. 2021;39(9):3225-34.
17. Joshi T, Joshi T, Sharma P, Mathpal S, Pundir H, Bhatt V, et al. In silico screening of natural compounds against COVID-19 by targeting Mpro and ACE2 using molecular docking. Eur Rev Med Pharmacol Sci. 2020;24(8):4529-36.
18. Bhuiyan FR, Howlader S, Raihan T, Hasan M. Plants Metabolites: Possibility of Natural Therapeutics Against the COVID-19 Pandemic. Front Med (Lausanne). 2020;7:444.
19. Santos-Buelga C, González-Paramás AM, Oludemi T, Ayuda-Durán B, González-Manzano S. Plant phenolics as functional food ingredients. Adv Food Nutr Res. 2019;90:183-257.
20. Gu L, Kelm MA, Hammerstone JF, Beecher G, Holden J, Haytowitz D, et al. Concentrations of proanthocyanidins in common foods and estimations of normal consumption. J Nutr. 2004;134(3):613-7.
21. Gu L, Kelm MA, Hammerstone JF, Beecher G, Holden J, Haytowitz D, et al. Screening of foods containing proanthocyanidins and their structural characterization using LC-MS/MS and thiolytic degradation. J Agric Food Chem. 2003;51(25):7513-21.
22. Nie Y, Stürzenbaum SR. Proanthocyanidins of Natural Origin: Molecular Mechanisms and Implications for Lipid Disorder and Aging-Associated Diseases. Adv Nutr. 2019;10(3):464-78.
23. Zhang L, Wang Y, Li D, Ho CT, Li J, Wan X. The absorption, distribution, metabolism and excretion of procyanidins. Food Funct. 2016;7(3):1273-81.
24. Dai J, Mumper RJ. Plant phenolics: extraction, analysis and their antioxidant and anticancer properties. Molecules. 2010;15(10):7313-52.
25. D'Archivio M, Filesi C, Di Benedetto R, Gargiulo R, Giovannini C, Masella R. Polyphenols, dietary sources and bioavailability. Ann Ist Super Sanita. 2007;43(4):348-61.
26. Russo M, Moccia S, Spagnuolo C, Tedesco I, Russo GL. Roles of flavonoids against coronavirus infection. Chem Biol Interact. 2020;328:109211.
27. Lalani S, Poh CL. Flavonoids as Antiviral Agents for Enterovirus A71 (EV-A71). Viruses. 2020;12(2).
28. Qian S, Fan W, Qian P, Zhang D, Wei Y, Chen H, et al. Apigenin restricts FMDV infection and inhibits viral IRES driven translational activity. Viruses. 2015;7(4):1613-26.
29. Steinmann J, Buer J, Pietschmann T, Steinmann E. Anti-infective properties of epigallocatechin-3-gallate (EGCG), a component of green tea. Br J Pharmacol. 2013;168(5):1059-73.
31. Li F, Song X, Su G, Wang Y, Wang Z, Jia J, et al. Amentoflavone Inhibits HSV-1 and ACV-Resistant Strain Infection by Suppressing Viral Early Infection. Viruses. 2019;11(5).
32. Lin YM, Anderson H, Flavin MT, Pai YH, Mata-Greenwood E, Pengsuparp T, et al. In vitro anti-HIV activity of biflavonoids isolated from Rhus succedanea and Garcinia multiflora. J Nat Prod. 1997;60(9):884-8.
33. Wehbe Z, Wehbe M, Iratni R, Pintus G, Zaraket H, Yassine HM, et al. Repurposing Ivermectin for COVID-19: Molecular Aspects and Therapeutic Possibilities. Front Immunol. 2021;12:663586.

34. Morris GM, Huey R, Lindstrom W, Sanner MF, Belew RK, Goodsell DS, et al. AutoDock4 and AutoDockTools4: Automated docking with selective receptor flexibility. J Comput Chem. 2009;30(16):2785-91.
35. Zali H, Golchin A, Farahani M, Yazdani M, Ranjbar MM, Dabbagh A. FDA Approved Drugs Repurposing of Toll-Like Receptor4 (TLR4) Candidate for Neuropathy. Iran J Pharm Res. 2019;18(3):1639-47.
36. Liu Z, Zhao J, Li W, Shen L, Huang S, Tang J, et al. Computational screen and experimental validation of anti-influenza effects of quercetin and chlorogenic acid from traditional Chinese medicine. Sci Rep. 2016;6:19095.
37. Crascì L, Basile L, Panico A, Puglia C, Bonina FP, Basile PM, et al. Correlating In Vitro Target-Oriented Screening and Docking: Inhibition of Matrix Metalloproteinases Activities by Flavonoids. Planta Med. 2017;83(11):901-11.
38. Jayaraj JM, Reteti E, Kesavan C, Muthusamy K. Structural insights on vitamin D receptor and screening of new potent agonist molecules: structure and ligand-based approach. J Biomol Struct Dyn. 2021;39(11):4148-59.
39. Azeez SA, Alhashim ZG, Al Otaibi WM, Alsuwat HS, Ibrahim AM, Almandil NB, et al. State-of-the-art tools to identify druggable protein ligand of SARS-CoV-2. Arch Med Sci. 2020;16(3):497-507.
40. Benalla W, Bellahcen S, Bnouham M. Antidiabetic medicinal plants as a source of alpha glucosidase inhibitors. Curr Diabetes Rev. 2010;6(4):247-54.
41. Lee C, Lee JM, Lee NR, Kim DE, Jeong YJ, Chong Y. Investigation of the pharmacophore space of Severe Acute Respiratory Syndrome coronavirus (SARS-CoV) NTPase/helicase by dihydroxychromone derivatives. Bioorg Med Chem Lett. 2009;19(16):4538-41.
42. Park HR, Yoon H, Kim MK, Lee SD, Chong Y. Synthesis and antiviral evaluation of 7-O-arylmethylquercetin derivatives against SARS-associated coronavirus (SCV) and hepatitis C virus (HCV). Arch Pharm Res. 2012;35(1):77-85.
43. Leung LK, Su Y, Chen R, Zhang Z, Huang Y, Chen ZY. Theaflavins in black tea and catechins in green tea are equally effective antioxidants. J Nutr. 2001;131(9):2248-51.
44. Babich H, Gold T, Gold R. Mediation of the in vitro cytotoxicity of green and black tea polyphenols by cobalt chloride. Toxicol Lett. 2005;155(1):195-205.
45. Babich H, Pinsky SM, Muskin ET, Zuckerbraun HL. In vitro cytotoxicity of a theaflavin mixture from black tea to malignant, immortalized, and normal cells from the human oral cavity. Toxicol In Vitro. 2006;20(5):677-88.
46. Decker EA. Phenolics: prooxidants or antioxidants? Nutr Rev. 1997;55(11 Pt 1):396-8.
47. Sakagami H, Arakawa H, Maeda M, Satoh K, Kadofuku T, Fukuchi K, et al. Production of hydrogen peroxide and methionine sulfoxide by epigallocatechin gallate and antioxidants. Anticancer Res. 2001;21(4a):2633-41.
48. Babich H, Gottesman RT, Liebling EJ, Schuck AG. Theaflavin-3-gallate and theaflavin-3'-gallate, polyphenols in black tea with prooxidant properties. Basic Clin Pharmacol Toxicol. 2008;103(1):66-74.
49. Narai-Kanayama A, Saruwatari K, Mori N, Nakayama T. Theaflavin-3-gallate specifically interacts with phosphatidylcholine, forming a precipitate resistant against the detergent action of bile salt. Biosci Biotechnol Biochem. 2018;82(3):466-75.
50. Clark KJ, Grant PG, Sarr AB, Belakere JR, Swaggerty CL, Phillips TD, et al. An in vitro study of theaflavins extracted from black tea to neutralize bovine rotavirus and bovine coronavirus infections. Vet Microbiol. 1998;63(2-4):147-57.
51. Lung J, Lin YS, Yang YH, Chou YL, Shu LH, Cheng YC, et al. The potential chemical structure of anti-SARS-CoV-2 RNA-dependent RNA polymerase. J Med Virol. 2020;92(6):693-7.
52. Zhang Z, Sun T, Niu JG, He ZQ, Liu Y, Wang F. Amentoflavone protects hippocampal neurons: anti-inflammatory, antioxidative, and antiapoptotic effects. Neural Regen Res. 2015;10(7):1125-33.
53. An J, Li Z, Dong Y, Ren J, Huo J. Amentoflavone protects against psoriasis-like skin lesion through suppression of NF-κB-mediated inflammation and keratinocyte proliferation. Mol Cell Biochem. 2016;413(1-2):87-95.
54. Liu H, Yue Q, He S. Amentoflavone suppresses tumor growth in ovarian cancer by modulating Skp2. Life Sci. 2017;189:96-105.
55. Ma SC, But PP, Ooi VE, He YH, Lee SH, Lee SF, et al. Antiviral amentoflavone from Selaginella sinensis. Biol Pharm Bull. 2001;24(3):311-2.
56. Lin YM, Flavin MT, Schure R, Chen FC, Sidwell R, Barnard DL, et al. Antiviral activities of biflavonoids. Planta Med. 1999;65(2):120-5.
57. Lee CW, Choi HJ, Kim HS, Kim DH, Chang IS, Moon HT, et al. Biflavonoids isolated from Selaginella tamariscina regulate the expression of matrix metalloproteinase in human skin fibroblasts. Bioorg Med Chem. 2008;16(2):732-8.
58. Pegnyemb DE, Mbing JN, de Théodore Atchadé A, Tih RG, Sondengam BL, Blond A, et al. Antimicrobial biflavonoids from the aerial parts of Ouratea sulcata. Phytochemistry. 2005;66(16):1922-6.
59. Kim HK, Son KH, Chang HW, Kang SS, Kim HP. Amentoflavone, a plant biflavone: a new potential anti-inflammatory agent. Arch Pharm Res. 1998;21(4):406-10.
60. Guruvayoorappan C, Kuttan G. Inhibition of tumor specific angiogenesis by amentoflavone. Biochemistry (Mosc). 2008;73(2):209-18.
61. Oh J, Rho HS, Yang Y, Yoon JY, Lee J, Hong YD, et al. Extracellular signal-regulated kinase is a direct target of the anti-inflammatory compound amentoflavone derived from Torreya nucifera. Mediators Inflamm. 2013;2013:761506.
62. Cao Q, Qin L, Huang F, Wang X, Yang L, Shi H, et al. Amentoflavone protects dopaminergic neurons in MPTP-induced Parkinson's disease model mice through PI3K/Akt and ERK signaling pathways. Toxicol Appl Pharmacol. 2017;319:80-90.
63. Rong S, Wan D, Fan Y, Liu S, Sun K, Huo J, et al. Amentoflavone Affects Epileptogenesis and Exerts Neuroprotective Effects by Inhibiting NLRP3 Inflammasome. Front Pharmacol. 2019;10:856.
64. Ryu YB, Jeong HJ, Kim JH, Kim YM, Park JY, Kim D, et al. Biflavonoids from Torreya nucifera displaying SARS-CoV 3CL(pro) inhibition. Bioorg Med Chem. 2010;18(22):7940-7.
66. Innocenti M, Michelozzi M, Giaccherini C, Ieri F, Vincieri FF, Mulinacci N. Flavonoids and biflavonoids in Tuscan berries of Juniperus communis L.: detection and quantitation by HPLC/DAD/ESI/MS. J Agric Food Chem. 2007;55(16):6596-602.
67. Liao S, Ren Q, Yang C, Zhang T, Li J, Wang X, et al. Liquid chromatography-tandem mass spectrometry determination and

pharmacokinetic analysis of amentoflavone and its conjugated metabolites in rats. J Agric Food Chem. 2015;63(7):1957-66.
68. Shen X, Niu X, Li G, Deng X, Wang J. Amentoflavone Ameliorates Streptococcus suis-Induced Infection In Vitro and In Vivo. Appl Environ Microbiol. 2018;84(24).
69. Wallace TC, Giusti MM. Evaluation of parameters that affect the 4-dimethylaminocinnamaldehyde assay for flavanols and proanthocyanidins. J Food Sci. 2010;75(7):C619-25.
70. Lee Y. Cancer Chemopreventive Potential of Procyanidin. Toxicol Res. 2017;33(4):273-82.
71. Rasmussen SE, Frederiksen H, Struntze Krogholm K, Poulsen L. Dietary proanthocyanidins: occurrence, dietary intake, bioavailability, and protection against cardiovascular disease. Mol Nutr Food Res. 2005;49(2):159-74.
72. De Taeye C, Caullet G, Eyamo Evina VJ, Collin S. Procyanidin A2 and Its Degradation Products in Raw, Fermented, and Roasted Cocoa. J Agric Food Chem. 2017;65(8):1715-23.
73. Khanal RC, Howard LR, Prior RL. Procyanidin content of grape seed and pomace, and total anthocyanin content of grape pomace as affected by extrusion processing. J Food Sci. 2009;74(6):H174-82.
74. Le Bourvellec C, Bagano Vilas Boas P, Lepercq P, Comtet-Marre S, Auffret P, Ruiz P, et al. Procyanidin-Cell Wall Interactions within Apple Matrices Decrease the Metabolization of Procyanidins by the Human Gut Microbiota and the Anti-Inflammatory Effect of the Resulting Microbial Metabolome In Vitro. Nutrients. 2019;11(3).
75. Zhuang M, Jiang H, Suzuki Y, Li X, Xiao P, Tanaka T, et al. Procyanidins and butanol extract of Cinnamomi Cortex inhibit SARS-CoV infection. Antiviral Res. 2009;82(1):73-81.